Int. J. Heat Mass Transfer. Vol. 35, No. 12, pp. 3407–3418, 1992
Printed in Great Britain

0017-9310/92 $5.00 + 0.00

Non-uniform porosity and thermal dispersion effects on natural convection about a heated horizontal cylinder in an enclosed porous medium

SHIH-WEN HSIAO
Industrial Design Department, National Cheng-Kung University, Tainan, Taiwan, R.O.C.

P. CHENG
Department of Mechanical Engineering, University of Hawaii, Honolulu, HI 96822, U.S.A.

and

CHAO-KUANG CHEN
Department of Mechanical Engineering, National Cheng-Kung University, Tainan, Taiwan, R.O.C.

(*Received* 5 *November* 1990 *and in final form* 20 *December* 1991)

Abstract—A numerical solution has been obtained for transient two-dimensional natural convection from a heated horizontal cylinder embedded in an enclosed porous medium. Non-Darcian effects are taken into consideration in the momentum equation, while the thermal dispersion effect is taken into consideration in the energy equation. The wall effect on porosity is approximated by an exponential function and its effect on thermal dispersion is modeled by a dispersive length. The governing equations in terms of the stream function, vorticity, and temperature are expressed in a body-fitted coordinate system, which were solved numerically by the finite difference method. Results are presented for the streamlines and isotherms, tangential velocity and temperature distributions, as well as the average Nusselt numbers at different values of Rayleigh number, dimensionless particle diameter, and Prandtl number. The non-uniform porosity effect tends to increase the temperature gradient near the wall while the thermal dispersion effect increases the effective thermal conductivity, both resulting in an increase in surface heat flux. The effect of thermal dispersion on natural convection in porous media at low to moderate Rayleigh number is small. With non-uniform porosity and thermal dispersion effects taken into consideration, the predicted average Nusselt numbers are found to be in better agreement with experimental data.

1. INTRODUCTION

In recent years the problem of natural convection about a heated horizontal cylinder embedded in a porous medium has attracted a great deal of attention because of its wide range of applications in engineering and geophysics [1–4]. Based on Darcy's law and boundary layer approximations, Merkin [1] obtained a similarity solution for natural convection about axisymmetric and two-dimensional bodies of arbitrary shape in a constant porosity medium of infinite extent at high Rayleigh numbers. Using the same approach, Cheng [2] has obtained a similarity solution for natural convection about a heated horizontal cylinder at uniform temperature, with the following expression for the average Nusselt number:

$$\overline{Nu}_m = 0.565 Ra_m^{1/2}. \quad (1)$$

In the above equation, $\overline{Nu}_m$ and Ra_m are the average media Nusselt number and the media Rayleigh number, which are defined as $\overline{Nu}_m = \bar{h}D/k_{m\infty}$ and $Ra_m = K_\infty \beta_f \rho_f D \Delta T^* / \mu_f \alpha_m$ respectively, where D is the diameter of the cylinder; $\bar{h}$ is the average heat transfer coefficient; g is the gravitational acceleration; β_f, ρ_f, and μ_f are the thermal expansion coefficient, density, and dynamic viscosity of the fluid respectively; ΔT^* is the difference between the wall temperature of the cylinder and the ambient temperature; $k_{m\infty}$, α_m and K_∞ are the stagnant thermal conductivity, the effective thermal diffusivity, and the permeability of the porous medium, which are assumed to be constant in deriving equation (1).

The first experimental investigation on natural convection about a horizontal cylinder (at uniform temperature) embedded in a porous medium was carried out by Fernandez and Schrock [3], who also performed a numerical solution of the problem based on the Darcy–Brinkman model in a constant porosity medium. Subsequently, Fand *et al.* [4] conducted a similar experimental investigation with different sizes of glass spheres saturated with water or silicone oil. A comparison of equation (1) with Fand *et al.*'s experimental data [4] shows that the measured media Nusselt numbers are higher than those predicted by theory [2].

Numerical and experimental investigations of natu-

NOMENCLATURE

A, B Ergun constants
B_0 constant defined in equation (7)
b dimensionless porous media shape parameter, $\varepsilon D^2/K$
C constant in equation (9a)
C_p specific heat at constant pressure
D cylinder diameter
Da Darcy number, K/D^2
d_p particle diameter
F inertial coefficient
g gravitational acceleration
H_1 height of the reservoir above the center of the cylinder
H_2 depth of the reservoir below the center of the cylinder
J Jacobian of coordinate transformation
K permeability
k_m thermal conductivity of the saturated media
l dispersive length
m the number of iteration
Nu_f fluid Nusselt number, hD/k_f
Nu_m media Nusselt number, hD/k_m
Pr Prandtl number
P, Q coordinate control functions
p pressure
q surface heat flux
Ra_m media Rayleigh number, $K_{m,x}\, g\beta_f D\Delta T^*/\nu_f\alpha_m$
Ra_f fluid Rayleigh number, $g\beta_f D^3\Delta T^*/\nu_f\alpha_f$
Ra_q media Rayleigh number for constant heat flux, $g\beta_f KDq/2\nu_f\alpha_m k_m$
Re_{ff} effective Rayleigh number defined by Himasekhar and Bau
r^*, r dimensional and dimensionless radial positions
r_d distance between the cylinder center and the top of the box
r_i distance between the cylinder center and the side walls
T^* dimensional temperature
T_h^*, T_c^* dimensional temperatures of the cylinder and the enclosure
t^* dimensional time
u^*, u dimensional and dimensionless Darcy velocity components in the x^*-direction
v^*, v dimensional and dimensionless Darcy velocity components in the y^*-direction
W half width of the reservoir
w^*, w dimensional and dimensionless absolute velocities
x^*, x dimensional and dimensionless horizontal coordinates
y^*, y dimensional and dimensionless vertical coordinates
∇ Laplace operator in the physical plane
$\tilde{\nabla}$ transformed Laplace operator given by equation (29d).

Greek symbols
α, β, δ transformation factors given by equation (25c)
α_f thermal diffusivity of fluid
α_m thermal diffusivity of the saturated porous medium
β_f thermal expansion coefficient of fluid
γ dimensionless particle diameter, d_p/D
ε porosity
Θ dimensionless temperature
θ angle measured from the upward vertical axis
μ_f dynamic viscosity of fluid
ν_f kinematic viscosity of fluid
ξ, η coordinates in the transformed plane
ρ_f density of fluid
ψ stream function
Ω vorticity
ω' modified vorticity.

Superscripts
$\bar{}$ average quantities
* dimensional.

Subscripts
f fluid phase
s solid phase.

ral convection about a heated horizontal cylinder with constant heat flux have recently been performed by Himasekhar and Bau [5]. They found that at high Rayleigh numbers, the measured average Nusselt numbers are higher than those obtained from their numerical solutions, which are based on the assumptions that Darcy's law is applicable, and the effects of variable porosity and thermal dispersion are negligible. The discrepancy between theory and experiments at high Rayleigh numbers is attributed to the transition to a three-dimensional, time-dependent flow that they observed in their experiments.

Similar discrepancies between theory and experiments have also been observed for natural convection heat transfer from other geometries embedded in a porous medium [2]. This discrepancy has prompted researchers to study other effects such as the non-uniform porosity and thermal dispersion, which were neglected in previous theoretical work. For example, the non-uniform porosity and thermal dispersion

effects in natural convection from a vertical flat plate in porous media have been investigated by Hong *et al.* [6], while the non-uniform porosity effect on natural convection in a cavity has been studied by David *et al.* [7]. It has been concluded that these effects become increasingly important when the ratio of the particle diameter to the characteristic length and the media Rayleigh number increases.

In this paper, the effects of non-uniform porosity and thermal dispersion on natural convection about a heated horizontal cylinder embedded in an enclosed porous medium are studied numerically. Both uniform wall temperature and uniform heat flux thermal boundary conditions on the cylinder are considered. The non-Darcian effects are taken into consideration in the momentum equation, while the thermal dispersion effect is taken into consideration in the energy equation. The wall effect on porosity is approximated by an exponential function and its effect on thermal dispersion is taken into consideration by a dispersive length concept proposed by Cheng *et al.* [7–9]. The governing dimensionless equations in terms of stream function, vorticity, and temperature are expressed in a body-fitted coordinate system, which was solved by the finite difference method. The streamlines and isotherms, tangential velocity and temperature distributions, as well as the local and average Nusselt numbers at different Rayleigh numbers, and dimensionless particle diameter are presented. It is found that the effects of non-uniform porosity and thermal dispersion tend to increase the surface heat flux. With these effects taken into consideration simultaneously, it is found that the predicted Nusselt numbers are in better agreement with experimental data [4, 5].

2. MATHEMATICAL FORMULATION

A horizontal circular cylinder of diameter D is embedded in an enclosed porous medium at T_c^* as shown in Fig. 1. The cylinder is suddenly heated at $t > 0$ and the convective heat transfer characteristics at $t > 0$ will be investigated. For a mathematical formulation of the problem, it is assumed that: (a) the saturated porous medium may be considered as a continuum, (b) the fluid flow and temperature distributions are two-dimensional, (c) the fluid and the solid particles are in local thermal equilibrium, and (d) the Boussinesq approximation is applicable. With these assumptions, the macroscopic conservation equations for convective heat transfer in a variable porosity medium are [8, 9]

$$\nabla \cdot v^* = 0 \tag{2}$$

$$\rho_f \left[\frac{\partial v^*}{\partial t^*} + \nabla \cdot \left(\frac{\bar{v}^* \bar{v}^*}{\varepsilon} \right) \right] = -\nabla p^* + \mu_f \nabla^2 \bar{v}^* - \frac{\mu_f \varepsilon \bar{v}^*}{K} - \rho_f \frac{F|\bar{v}^*|\bar{v}^* \varepsilon}{\sqrt{K}} + \rho_f \beta_f (T^* - T^*_\infty) \varepsilon \bar{g} \tag{3}$$

and

$$\frac{\partial}{\partial t^*}[(\rho C_p)_f \varepsilon + (\rho C_p)_s (1-\varepsilon)] T^* + (\rho C_p)_f \nabla \cdot (\bar{v}^* T^*) = \nabla \cdot [k_e \nabla T^*] \tag{4}$$

where $\bar{v}^*$ and p^* are the volume-averaged velocity vector and pressure; C_{pf} and C_{ps} are the specific heats of fluids and solid phases at constant pressure; F is the inertial coefficient; ε is the porosity, and k_e is the effective thermal conductivity of the saturated porous medium, which is a superposition of the stagnant thermal conductivity (k_m) and the dispersive conductivity (k_d), i.e. $k_e = k_m + k_d$.

For a porous medium composed of packed spheres, the porosity ε varies from 0.36 far from the wall to nearly unity at the wall. As shown by Vortmeyer and Schuster [10], the variation of the porosity can be approximated by an exponential function of the form

$$\varepsilon = \varepsilon_\infty + (\varepsilon_0 - \varepsilon_\infty)\, e^{-N_1 (r^* - r_0^*)/d_p} \tag{5}$$

where d_p is the particle diameter, r^* is the radial coordinate and r_0^* is the radius of the cylinder; ε_∞ and ε_0 are the porosities at a location far away and on the wall while N_1 is an empirical constant. $N_1 = 2$ was used by most previous investigators [10]. Recently, some investigators have suggested that a value of $N_1 = 5$–7 should be used instead [8, 9, 11, 12].

For a packed-sphere bed, the permeability and the Forchhemier coefficient are related to the porosity by

$$K = \frac{d_p^2 \varepsilon^3}{A(1-\varepsilon)^2} \quad \text{and} \quad F = \frac{B}{\sqrt{A}\varepsilon^{3/2}} \tag{6}$$

where A and B are empirical constants. Ergun [13] found that $A = 150$ and $B = 1.75$, while Macdonald *et al.* [14] found that $A = 182$ and $B = 1.92$. Most recently, Fand *et al.* [15] performed some experiments on pressure drop in tubes packed with different sizes of glass spheres, and determined that $A = 182$ and $B = 1.92$ based on the Ergun equation with a constant porosity equal to 0.36. In a recent paper, Cheng *et al.* [12] reanalyzed Fand *et al.*'s data based on a hydrodynamically fully developed flow in a packed tube with a variable porosity model; they found that the

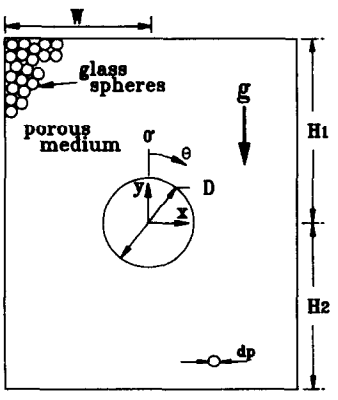

FIG. 1. Physical model and coordinate system.

calculated pressure drop matches with Fand *et al.*'s data if the values of $A = 215$ and $B = 1.92$ are used in equation (6).

The value of the stagnant thermal conductivity of the saturated porous medium can be computed according to the following expression, given by Zehner and Schluender [16] as

$$\frac{k_m}{k_f} = (1-\sqrt{(1-\varepsilon)}) + \frac{2\sqrt{(1-\varepsilon)}}{1-\lambda B_0} \times \left[\frac{(1-\lambda)B_0}{(1-\lambda B_0)^2}\ln\left(\frac{1}{\lambda B_0}\right) - \frac{B_0+1}{2} - \frac{B_0-1}{1-\lambda B_0}\right] \quad (7)$$

where $B_0 = 1.25\,[(1-\varepsilon)/\varepsilon]^{10/9}$ and $\lambda = k_f/k_s$ with k_f and k_s denoting the thermal conductivity of the fluid and the solid phase respectively. The value of k_s for the glass beads is calculated based on the following expression [17]:

$$k_s = 1.00416 + 1.6736\times10^{-3}T^* - 4.184\times10^{-6}T^{*2} \quad (8)$$

where T^* is the temperature in °C and k_s is expressed in W m^{-1} °C^{-1}.

The thermal dispersion conductivity for flow through a porous medium is given by [8, 9]

$$k_d = C(\rho C_p)_f |\bar{w}| l d_p \quad (9a)$$

where l is the dispersive length, which is given by

$$l = \frac{1-\varepsilon}{\varepsilon} \quad (9b)$$

while $w^* = (u^{*2}+v^{*2})^{1/2}$ and the value of the dispersivity $C = 0.02$–0.04 was determined by a comparison of theory and experiments for forced convection in packed columns [8, 9]. Equations (2)–(9) are the governing equations for natural convection in a non-uniform porosity medium.

Consider first the case where the wall temperature of the cylinder is suddenly raised to T_h^*. For this case, we introduce the following dimensionless variables:

$$x = x^*/D,\quad y = y^*/D,\quad u = u^*D/\alpha_f,\quad v = v^*D/\alpha_f,$$
$$\Theta = \frac{T^*-T_c^*}{T_h^*-T_c^*},\quad t = \frac{\alpha_f t^*}{D^2},\quad P = p^*D^2/\rho_f\alpha_f^2 \quad (10)$$

where D is the diameter of the cylinder, α_f is the thermal diffusivity of the fluid, and T_h^*, T_c^* are the temperatures of the cylinder and the enclosure respectively. In terms of the dimensionless variables, equations (2)–(9) become

$$\frac{\partial u}{\partial x} + \frac{\partial v}{\partial y} = 0 \quad (11)$$

$$\frac{\partial u}{\partial t} + u\frac{\partial}{\partial x}\left(\frac{u}{\varepsilon}\right) + v\frac{\partial}{\partial y}\left(\frac{u}{\varepsilon}\right) = -\frac{\partial P}{\partial x} + Pr_f\nabla^2 u - \left(\frac{Pr_f}{Da} + \frac{F}{\sqrt{(Da)}}|\bar{w}|\right)\varepsilon u \quad (12)$$

$$\frac{\partial v}{\partial t} + u\frac{\partial}{\partial x}\left(\frac{v}{\varepsilon}\right) + v\frac{\partial}{\partial y}\left(\frac{v}{\varepsilon}\right) = -\frac{\partial P}{\partial y} + Pr_f\nabla^2 v - \left(\frac{Pr_f}{Da} + \frac{F}{\sqrt{(Da)}}|\bar{w}|\right)\varepsilon v + Ra_f\,Pr_f\,\varepsilon\Theta \quad (13)$$

$$\frac{\partial}{\partial t}(\sigma\Theta) + u\frac{\partial\Theta}{\partial x} + v\frac{\partial\Theta}{\partial y} = \frac{\partial}{\partial x}\left(\frac{\alpha_e}{\alpha_f}\frac{\partial\Theta}{\partial x}\right) + \frac{\partial}{\partial y}\left(\frac{\alpha_e}{\alpha_f}\frac{\partial\Theta}{\partial y}\right) \quad (14)$$

where σ, α_e, Pr_f, and Ra_f are the heat capacity ratio of the saturated porous medium to that of the fluid, the effective thermal diffusivity of the saturated porous medium, the Prandtl number, and the fluid Rayleigh number, which are defined as

$$\sigma = \frac{(\rho C_p)_f\varepsilon + (\rho C_p)_s(1-\varepsilon)}{(\rho C_p)_f},\quad \alpha_e = \frac{k_e}{(\rho C_p)_f} \quad (15a)$$
$$Pr_f = \frac{\nu_f}{\alpha_f},\quad Ra_f = \frac{g\beta_f(T_h^*-T_c^*)D^3}{\alpha_f\nu_f}$$

where

$$Ra_f = Ra_m\,Da_{\gamma\gamma}(\alpha_m/\alpha_f)$$

with $Da_{\gamma\gamma}$ being the bulk Darcy number, defined as

$$Da_{\gamma\gamma} = K_{\gamma\gamma}/D^2 = \frac{\gamma^2\varepsilon_{\gamma\gamma}^3}{A(1-\varepsilon_{\gamma\gamma})^2} \quad (15b)$$

where $\gamma = d_p/D$ is the dimensionless particle diameter. The local Darcy number (Da) is related to the bulk Darcy number ($Da_{\gamma\gamma}$) by

$$Da = Da_{\gamma\gamma}\frac{K}{K_{\gamma\gamma}} = Da_{\gamma\gamma}\left(\frac{\varepsilon}{\varepsilon_{\gamma\gamma}}\right)^3\left(\frac{1-\varepsilon_{\gamma\gamma}}{1-\varepsilon}\right)^2. \quad (15c)$$

Note that the inertial terms in equations (12) and (13) are important if the local value of $F\sqrt{(Da)}/Pr_f \gg 1$. This implies that the inertial term may be important near the wall, although it may be negligible away from the wall. Eliminating the pressure terms in equations (12) and (13), we can express the resulting equations in terms of stream function and vorticity as

$$\nabla^2\psi = -\Omega \quad (16)$$

$$\frac{\partial\Omega}{\partial t} + \frac{\partial\psi}{\partial y}\left[\frac{\partial\omega}{\partial x} - \frac{\partial}{\partial x}\left(\frac{1}{\varepsilon}\right)\frac{\partial^2\psi}{\partial y^2} + \frac{\partial}{\partial y}\left(\frac{1}{\varepsilon}\right)\frac{\partial^2\psi}{\partial y^2}\right] - \frac{\partial\psi}{\partial x}\left[\frac{\partial\omega}{\partial y} + \frac{\partial}{\partial x}\left(\frac{1}{\varepsilon}\right)\frac{\partial^2\psi}{\partial x\,\partial y} - \frac{\partial}{\partial y}\left(\frac{1}{\varepsilon}\right)\frac{\partial^2\psi}{\partial x^2}\right]$$
$$= Pr_f\nabla^2\Omega - \left[\left(\frac{Pr_f}{Da} + \frac{F}{\sqrt{(Da)}}|\bar{w}|\varepsilon\right)\right]\Omega + \frac{\partial\psi}{\partial y}\frac{\partial}{\partial y}\left[\left(\frac{Pr_f}{Da} + \frac{F}{\sqrt{(Da)}}w\right)\varepsilon\right] + \frac{\partial\psi}{\partial x}\frac{\partial}{\partial x}\left[\left(\frac{Pr_f}{Da} + \frac{F}{\sqrt{(Da)}}|\bar{w}|\varepsilon\right)\right] + Ra_f\,Pr_f\frac{\partial}{\partial x}(\varepsilon\Theta) \quad (17)$$

$$\sigma\frac{\partial\Theta}{\partial t}+\frac{\partial\psi}{\partial y}\frac{\partial\Theta}{\partial x}-\frac{\partial\psi}{\partial x}\frac{\partial\Theta}{\partial y}=\frac{\alpha_e}{\alpha_f}\nabla^2\Theta + \frac{\partial}{\partial x}\left(\frac{\alpha_e}{\alpha_f}\frac{\partial\Theta}{\partial x}\right)+\frac{\partial}{\partial y}\left(\frac{\alpha_e}{\alpha_f}\frac{\partial\Theta}{\partial y}\right) \quad (18)$$

where the dimensionless stream function, vorticity function, and the modified vorticity function are defined as

$$u=\frac{\partial\psi}{\partial y},\quad v=-\frac{\partial\psi}{\partial x},$$

$$\Omega=\frac{\partial v}{\partial x}-\frac{\partial u}{\partial y},$$

$$\omega=\frac{\partial}{\partial x}\left(\frac{v}{\varepsilon}\right)-\frac{\partial}{\partial y}\left(\frac{u}{\varepsilon}\right). \quad (19)$$

Initially, the cylinder and the porous medium are at a uniform temperature T_c^*. Thus, the initial conditions of the problem are

$$\psi=\Omega=\Theta=0,\quad \text{at}\quad t=0. \quad (20a\text{–}c)$$

The boundary conditions on the cylinder are

$$\psi=0,\quad \Theta=1,\quad \Omega=-\psi_{rr},\quad \text{at}\quad r^*=r_0^* \quad (21a\text{–}c)$$

while on the wall of the container they are

$$\psi=\Theta=0,\quad \Omega=-\psi_{yy}\quad \text{on the vertical walls} \quad (22a\text{–}c)$$

$$\psi=\Theta=0,\quad \Omega=-\psi_{yy}\quad \text{on the horizontal walls} \quad (23a\text{–}c)$$

where r_0^* is the radius of the cylinder.

3. NUMERICAL PROCEDURE

We now express the governing equations in terms of a body-fitted coordinate system. This can be achieved based on the method of automatic generation of curvilinear coordinates developed by Thompson *et al.* [18]. The boundary-fitted physical coordinate system is created by solving the following system of Poisson equations:

$$\nabla^2\xi=P(\xi,\eta) \quad (24a)$$

$$\nabla^2\xi=P(\xi,\eta) \quad (24b)$$

where P and Q are the coordinate control functions that provide the control of the mesh concentration [19, 20]. Since it is desirable to perform all numerical calculations in the transformed plane, the dependent and independent variables must be interchanged in equations (24a) and (24b). The transformed equations are

$$\alpha x_{\xi\xi}-2\beta x_{\xi\eta}+\delta x_{\eta\eta}+J^2(Px_\xi+Qx_\eta)=0 \quad (25a)$$

$$\alpha y_{\xi\xi}-2\beta y_{\xi\eta}+\delta y_{\eta\eta}+J^2(Py_\xi+Qy_\eta)=0 \quad (25b)$$

where

$$\alpha=x_\eta^2+y_\eta^2,\quad \beta=x_\xi x_\eta+y_\xi y_\eta,$$

$$\delta=x_\xi^2+y_\xi^2,\quad J=x_\xi y_\eta+x_\eta y_\xi. \quad (25c)$$

Note that the values of x and y on the boundaries of the (ξ,η) domain are prescribed.

The transformed equations (25) are discretized over the mathematical plane using second-order central difference, and the resulting finite difference equations are solved with the successive over-relaxation (SOR) method. Once a grid is generated, the values of the coefficients α, β, δ, and J, etc. are evaluated and stored for use in the solution of the governing equations.

The governing equations (16)–(18) in terms of the transformed coordinates are

$$\tilde\nabla^2\psi=-\Omega \quad (26)$$

$$\frac{\partial\Omega}{\partial t}+\frac{1}{J}(\psi_\eta w_\xi-\psi_\xi w_\eta)=Pr_f\,\tilde\nabla^2\Omega - \left[\left(\frac{Pr_f}{Da}+\frac{F}{\sqrt{(Da)}}|\bar v|\right)\varepsilon\right]\Omega+\frac{1}{J^2}(x_\xi\psi_\eta-x_\eta\psi_\xi) \times\left\{x_\xi\left[\left(\frac{Pr_f}{Da}+\frac{F}{\sqrt{(Da)}}|\bar v|\right)\varepsilon\right]_\eta - x_\eta\left[\left(\frac{Pr_f}{Da}+\frac{F}{\sqrt{(Da)}}|\bar v|\right)\varepsilon\right]_\xi\right\} + \frac{1}{J^2}(y_\eta\psi_\xi-y_\xi\psi_\eta)\left\{y_\eta\left[\left(\frac{Pr_f}{Da}+\frac{F}{\sqrt{(Da)}}|\bar v|\right)\varepsilon\right]_\xi - y_\xi\left[\left(\frac{Pr_f}{Da}+\frac{F}{\sqrt{(Da)}}|\bar v|\right)\varepsilon\right]_\eta\right\} + \frac{Ra_f\,Pr_f}{J}[y_\eta(\varepsilon\Theta)_\xi-y_\xi(\varepsilon\Theta)_\eta] + \frac{u}{J^2}\left\{\left[y_\eta\left(\frac{1}{\varepsilon}\right)_\xi-y_\xi\left(\frac{1}{\varepsilon}\right)_\eta\right](x_\xi u_\eta-x_\eta u_\xi) + \left[x_\xi\left(\frac{1}{\varepsilon}\right)_\eta-x_\eta\left(\frac{1}{\varepsilon}\right)_\xi\right](x_\xi v_\eta-x_\eta v_\xi)\right\} - \frac{v}{J^2}\left\{\left[y_\eta\left(\frac{1}{\varepsilon}\right)_\xi-y_\xi\left(\frac{1}{\varepsilon}\right)_\eta\right](y_\eta u_\xi-y_\xi u_\eta) + \left[x_\xi\left(\frac{1}{\varepsilon}\right)_\eta-x_\eta\left(\frac{1}{\varepsilon}\right)_\xi\right](y_\eta v_\xi-y_\xi v_\eta)\right\} \quad (27)$$

and

$$\sigma\frac{\partial\Theta}{\partial t}+\frac{1}{J}(\psi_\eta\Theta_\xi-\psi_\xi\Theta_\eta)=\frac{\alpha_e}{\alpha_f}\tilde\nabla^2\Theta + \frac{1}{J^2}(y_\eta\Theta_\xi-y_\xi\Theta_\eta)\left[y_\eta\left(\frac{\alpha_e}{\alpha_f}\right)_\xi-y_\xi\left(\frac{\alpha_e}{\alpha_f}\right)_\eta\right] + \frac{1}{J^2}(x_\xi\Theta_\eta-x_\eta\Theta_\xi)\left[x_\xi\left(\frac{\alpha_e}{\alpha_f}\right)_\eta-x_\eta\left(\frac{\alpha_e}{\alpha_f}\right)_\xi\right] \quad (28)$$

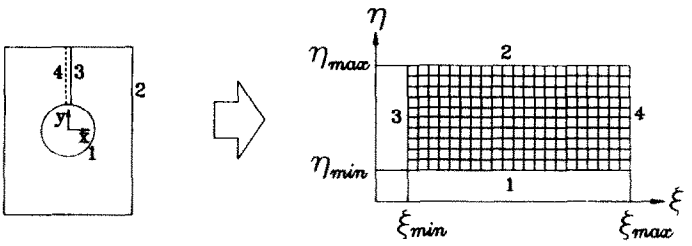

FIG. 2. Coordinate transformation.

where u, v, and w are given by

$$u = (x_\xi \psi_\eta - \chi_\eta \psi_\xi)/J \tag{29a}$$

$$v = (y_\xi \psi_\eta - y_\eta \psi_\xi)/J \tag{29b}$$

$$|w| = \frac{1}{J}[(x_\xi \psi_\eta - x_\eta \psi_\xi)^2 + (y_\xi \psi_\eta - y_\eta \psi_\xi)^2]^{1/2}. \tag{29c}$$

The transformed Laplace operator in equations (26) and (28) is

$$\tilde{\nabla}^2 = [\alpha \partial_{\xi\xi} - 2\beta \partial_{\xi\eta} + \delta \partial_{\eta\eta} + J^2(P \partial_\xi - Q \partial_\eta)]/J^2. \tag{29d}$$

In terms of the transformed coordinates, the boundary conditions become

$$\eta = \eta_{\min}: \quad \psi = 0, \quad \Theta = 1, \quad \Omega = -\delta \psi_{\eta\eta}/J^2 \tag{30a}$$

$$\eta = \eta_{\max}: \quad \psi = 0, \quad \Theta = 1, \quad \Omega = -\delta \psi_{\eta\eta}/J^2 \tag{30b}$$

where $\eta_{\min}$ and $\eta_{\max}$ are the inner and outer boundaries in the transformed plane (Fig. 2), respectively.

Equations (26)–(30) are discretized based on the finite difference method. A first-order forward difference approximation is used for the time derivative and a second-order central difference approximation is used for space derivatives. Finite difference equations for the stream function were solved by the successive over-relaxation method (SOR), while those for vorticity and temperature were solved by the alternating direction implicit (ADI) method. The mesh size required for a sufficiently accurate numerical solution depends on the values of the Rayleigh number and the Darcy number. A coarse grid was initially used and the grid size was gradually reduced until the value of the Nusselt number did not change in the third significant figure. It was found a grid of 65×80 (see Fig. 3) to be sufficiently accurate. All computations were performed with a time increment of $\Delta t = 10^{-4}$.

The convergence criterion used for stream function, vorticity, and temperature is

$$\left| \frac{f^m - f^{m-1}}{f^{m-1}} \right| < 10^{-4} \tag{31}$$

where f denotes ψ, Ω or Θ, while m is the number of the iteration. After convergence of the numerical solution has been achieved, the local and the mean fluid Nusselt numbers (Nu_f and $\overline{Nu}_f$) can be calculated as

$$Nu_f = \frac{hD}{k_f} = -\left(\frac{\partial \Theta}{\partial r}\right)_{r=1} \tag{32a}$$

$$\overline{Nu}_f = \frac{1}{\pi}\int_0^\pi Nu_f \, d\theta \tag{32b}$$

where θ is measured clockwise from the upward vertical axis. The local and average media Nusselt numbers are defined as

$$Nu_m = \frac{hD}{k_{m,\infty}}, \quad \overline{Nu}_m = \frac{1}{\pi}\int_0^\pi Nu_m \, d\theta. \tag{33}$$

It follows that

$$Nu_m = \frac{k_f}{k_{m,\infty}} Nu_f \quad \text{and} \quad \overline{Nu}_m = \frac{k_f}{k_{m,\infty}} \overline{Nu}_f. \tag{34}$$

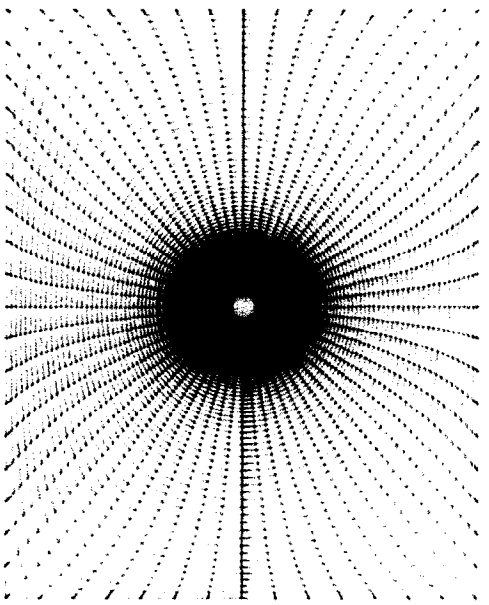

FIG. 3. A typical grid of 65×80 nodal points.

Table 1. Values of Ra_f and Ra_m used in the numerical computations

d_p (mm)	γ	$Ra_m = 15$	$Ra_m = 273$	$Ra_f = 10^6$
2	0.175	$Ra_f = 9.3 \times 10^5$	$Ra_f = 1.69 \times 10^7$	$Ra_m = 16.1$
3	0.262	$Ra_f = 3.9 \times 10^5$	$Ra_f = 7.18 \times 10^6$	$Ra_m = 38.0$
4	0.349	$Ra_f = 2.3 \times 10^5$	$Ra_f = 4.23 \times 10^6$	$Ra_m = 64.5$
6	0.524	$Ra_f = 1.03 \times 10^5$	$Ra_f = 1.88 \times 10^6$	$Ra_m = 145.0$

4. COMPARISON WITH FAND *et al.*'s DATA [4]

The parameters shown in the governing equations given by equations (16)–(18) and boundary conditions given by equations (20)–(22) are H_1/D, H_2/D, W/D, Ra_f, Pr_f, λ, σ, and Da_∞ (or γ). In addition, the values of empirical constants ε_∞, ε_0, N_1, A and B must be prescribed. All of the numerical results presented graphically in this paper were calculated with $\varepsilon_\infty = 0.36$, $\varepsilon_0 = 0.9$, $N_1 = 7$, $A = 215$ and $B = 1.92$. A parametric study with different values of other parameters was performed, and the results for surface heat flux will be presented either in terms of fluid Nusselt number ($\overline{Nu}_f$) or media Nusselt number ($\overline{Nu}_m$) vs fluid Rayleigh number (Ra_f) or media Rayleigh number (Ra_m), whichever is appropriate. Computations were also carried out for the cases corresponding to Fand *et al.*'s experimental conditions. Table 1 lists the values of Ra_f corresponding to $Ra_m = 15$ and 273 for $D = 11.45$ mm and different sizes of glass spheres saturated with water, which were used in Fand *et al.*'s experiments [4]. The following symbols are used in the presentation of results: VPWD stands for variable porosity with thermal dispersion effect, while VPND stands for variable porosity without thermal dispersion effect; CPWD stands for constant porosity with thermal dispersion effect, while CPND stands for constant porosity without thermal dispersion effect.

Natural convection in a constant-porosity medium

Numerical results will first be presented for natural convection about a heated horizontal cylinder embedded in an infinite medium of constant porosity. From experimental observations, Fand *et al.* [4] have concluded that the enclosed medium shown in Fig. 1 can be considered as infinite if $H_1/D = H_2D = 11.1$ and $W/D = 8.8$. In order to check this conclusion, computations were carried out for this size of enclosure as well as for $H_1/D = H_2/D = 22.2$ and $W/D = 8.8$ (with $D = 11.45$ mm) for water ($Pr_f = 3.2$) and glass beads (with $d_p = 3$ mm) at different Rayleigh numbers with and without thermal dispersion effects taken into consideration. The results of the computation for the average Nusselt number with thermal dispersion effects as a function of time are presented in Fig. 4. It can be seen that (a) no noticeable differences in the mean Nusselt numbers are observed between the two sizes of the enclosure, which confirms Fand *et al.*'s observation [4] that the measured Nusselt numbers are independent of the enclosure size, implying an infinite porous medium, and (b) the time to reach steady state increases as the Rayleigh number is decreased. For example, the times required to reach steady state for a water/glass beads system are 248 s at $Ra_m = 273$ and 450 s at $Ra_m = 15$.

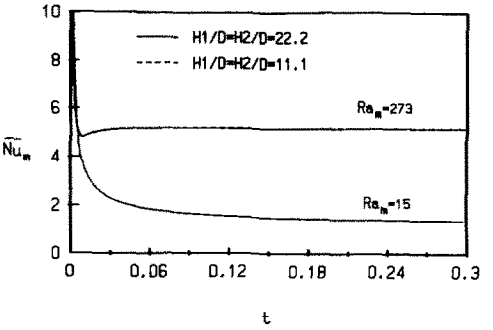

FIG. 4. Effects of reservoir height and depth on transient Nusselt number variations based on the CPWD model.

The effects of dimensionless particle diameter, thermal dispersion and no-slip boundary condition on the steady average media Nusselt number as a function of the media Rayleigh number in a constant porosity medium are shown in Fig. 5. Results based on Darcy's law without boundary layer approximation and thermal dispersion are represented by dashed lines with $\gamma = 0$. Results for $\gamma = 0.184$ and 0.522 based on the Darcy–Brinkman model with and without thermal dispersion are also presented for comparison purposes. It is relevant to note that the assumption of a continuum may not be valid for the case $\gamma = 0.522$. From this figure, it can be concluded that (1) the boundary layer approximation is valid if $Ra_m > 30$, (2) the thermal dispersion effect is important only

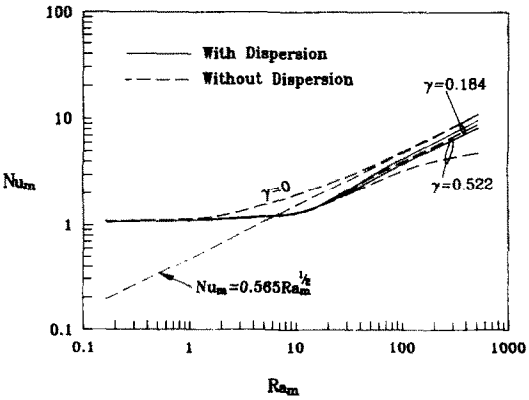

FIG. 5. Effects of thermal dispersion on steady average Nusselt number based on the CPWD and CPND models.

at high Rayleigh numbers with a high dimensionless particle diameter, and (3) the onset of free convection begins at $Ra_m = 1.9$ in a constant porosity medium if Darcy's law is used as the momentum equation.

Natural convection in a non-uniform porosity medium

To find the effects of the empirical constants A and B on the Nusselt number, computations were carried out based on the VPWD model with the values of A and B given by Ergun [13], Macdonald *et al.* [14], Fand *et al.* [15] and Cheng *et al.* [12]. Results of the computations for the average media Nusselt number ($\overline{Nu}_m$) are listed in columns 6–8 of Table 2, which shows that (1) the effect of the values of A and B on the calculated Nusselt numbers is small, and (2) the calculated Nusselt numbers based on $A = 215$ and $B = 1.92$ are closest to Fand *et al.*'s experimental data. Note that Fand *et al.*'s experimental data for the media Nusselt number were evaluated based on the definition that $\overline{Nu}_{Fm} = \bar{h}D/k_c$ with $k_c = \varepsilon k_f + (1-\varepsilon)k_s$. It follows that $\overline{Nu}_m = \overline{Nu}_{Fm}(k_c/k_{m,r})$ and Fand *et al.*'s data in terms of $\overline{Nu}_m$ are listed in Table 2.

To investigate the effects of reservoir width on the heat transfer rate from the horizontal heated cylinder embedded in a variable porosity medium, computations were also carried out for smaller values of W/D while keeping $H_1/D = H_2/D = 11.1$. The results of the computation for the steady average fluid Nusselt number ($\overline{Nu}_f$) are presented in Fig. 6, which shows that the value of $\overline{Nu}_f$ decreases as the value of W/D decreases from 11.1.

Figure 7 is a comparison of the measured Nusselt numbers ($\overline{Nu}_f$) for $d_p = 3$ mm and the calculated Nusselt numbers based on four theoretical models. It is shown that the effect of thermal dispersion increases the heat transfer rate for both constant porosity and variable porosity models. The values of the Nusselt number based on the constant porosity model are below experimental data. The results of the variable porosity model with thermal dispersion (VPWD) taken into consideration agree the best with experimental data. The effects of thermal dispersion, however, are small in constant and variable porosity models.

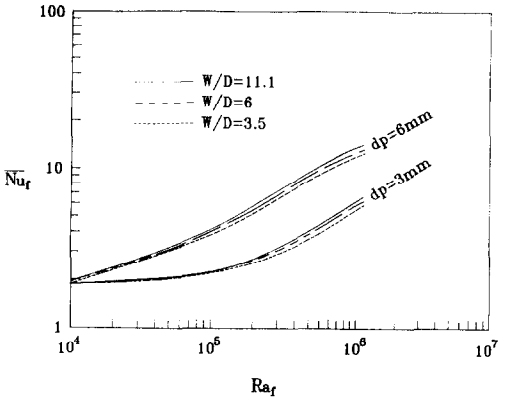

FIG. 6. Effects of reservoir width on steady Nusselt number based on the VPWD model.

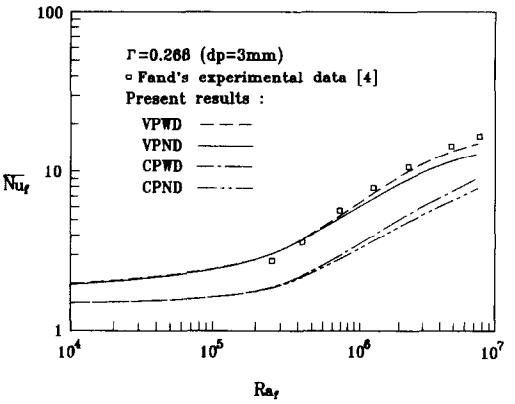

FIG. 7. A comparison of measured and calculated steady Nusselt numbers based on four models.

Figure 8(a) shows a comparison of Fand *et al.*'s measured Nusselt numbers for $d_p = 4$ mm and 2 mm with calculated Nusselt numbers based on the VPWD model. The results for $d_p = 3$ mm presented in Fig. 7

Table 2. A comparison of calculated Nusselt numbers with Fand *et al.*'s [4] experimental results ($\gamma = 0.262$)

			Present code					
			Constant porosity without dispersion no-slip $\varepsilon = 0.36$ $A = 215$ $B = 1.92$	Variable porosity without dispersion no-slip $\varepsilon_w = 0.9$, $\varepsilon_\infty = 0.36$, $A = 215$, $B = 1.92$	Variable porosity with dispersion no-slip $\varepsilon_w = 0.9$, $\varepsilon_\infty = 0.36$			
Cases	Ra_m	Pr_f			$A = 150$ $B = 1.75$	$A = 182$ $B = 1.92$	$A = 215$ $B = 1.92$	Fand *et al.*'s experimental data [4]
1w3†	7.82	6.02	1.396	1.56	1.716	1.741	1.764	1.914
2w3†	12.75	5.78	1.583	2.02	2.283	2.302	2.321	2.546
3w3†	23.52	5.38	2.744	3.43	3.739	3.793	3.848	3.986
4w3†	41.78	4.87	3.842	4.95	5.261	5.335	5.409	5.537
5w3†	77.13	4.38	5.334	6.34	6.856	7.071	7.286	7.509
6w3†	154.62	3.64	7.126	8.43	9.251	9.376	9.502	10.103
7w3†	240.72	3.19	8.105	9.62	10.345	10.48	10.723	11.747

† The first digit indicates the test number; w = water; the final digit indicates the nominal glass sphere diameter (mm).

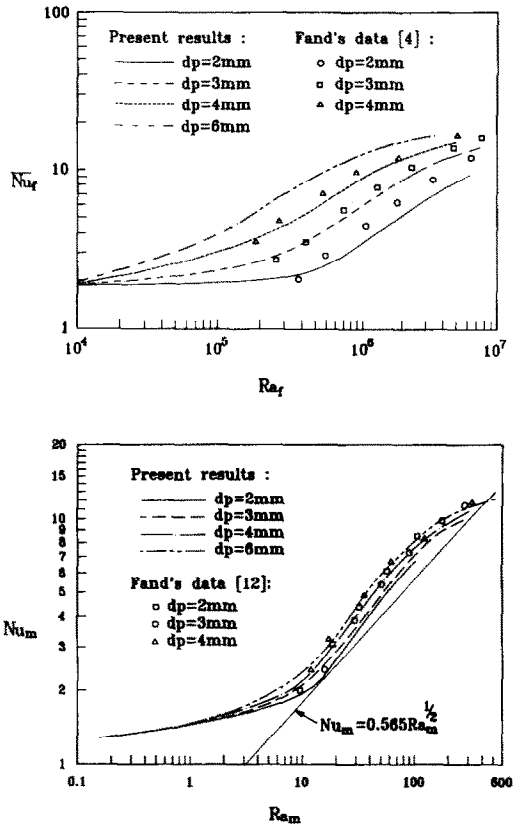

FIG. 8. A comparison of measured and calculated steady Nusselt numbers of a horizontal cylinder embedded in an infinite porous medium: (a) $\overline{Nu}_f$ vs Ra_f; (b) $\overline{Nu}_m$ vs Ra_m.

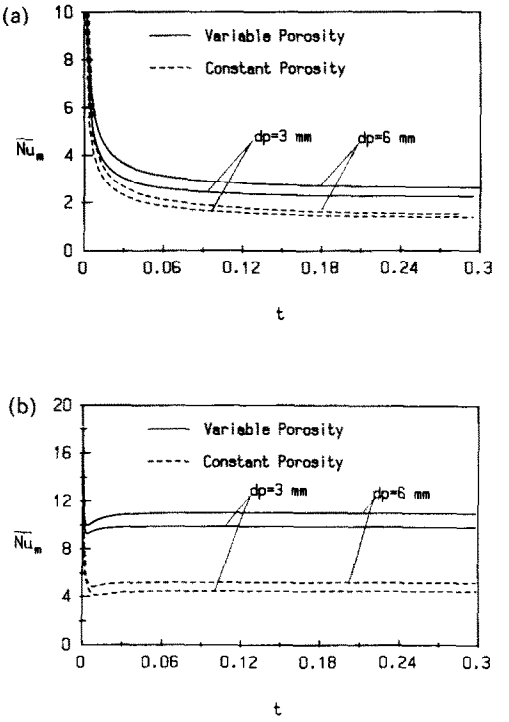

FIG. 9. Effects of variable porosity and particle diameter on transient average Nusselt number based on the CPWD and VPWD models: (a) $Ra_m = 15$; (b) $Ra_m = 273$.

are also plotted for comparison purposes. The results in Fig. 8(a) are replotted in terms of the media Nusselt number vs the media Rayleigh number in Fig. 8(b). It is shown that (1) the predicted average Nusselt numbers with variable porosity and thermal dispersion effects taken into consideration agree with experimental data, (2) the Nusselt number in the convection regime increases as the particle diameter is increased, and (3) the Nusselt number in the conduction regime is relatively independent of the particle diameter.

The effects of variable porosity and particle diameter on the average media Nusselt number ($\overline{Nu}_m$) as a function of time are depicted in Fig. 9(a) for $Ra_m = 15$ and in Fig. 9(b) for $Ra_m = 273$. It can be seen that the variable porosity effect is negligible at small times and its influence increases with particle diameter and Rayleigh number.

The effects of variable porosity and thermal dispersion on the tangential velocity and temperature profiles are shown in Fig. 10 for $Ra_m = 247$, $Pr_f = 3.2$, and $d_p = 3$ mm at $\theta = 45°$. It is shown that both the variable porosity and thermal dispersion effects increase the tangential velocity and the temperature gradient, leading to an enhancement of surface heat flux. The variable porosity effect tends to reduce the thermal boundary layer thickness while the thermal

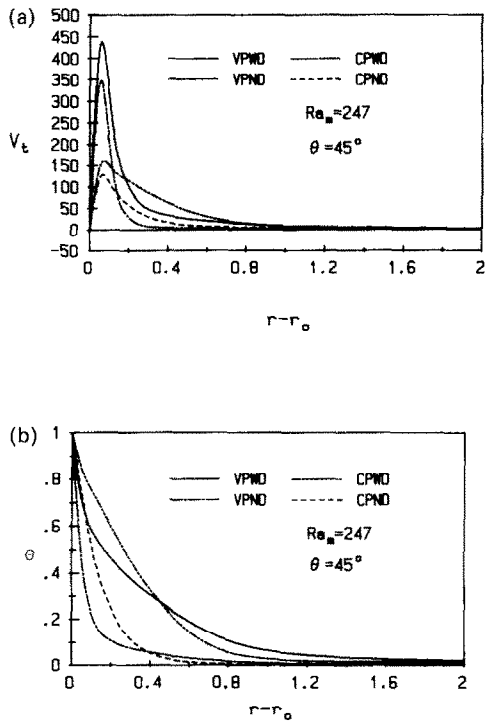

FIG. 10. Effects of variable porosity and thermal dispersion on tangential velocity (a) and temperature distribution (b).

Table 3. Comparison of numerical results for $Ra_m = 50$ with $H_1 = 7.4$ and $H_2 = 14.6$

Source	Himasekhar and Bau's numerical solution [5]	Present code
Number of grid points	50×50	65×70
Nu_i	4.442	4.453
Nu_0	4.444	4.458
ψ_{max}	9.61	9.59

dispersion has the opposite effect. Thus, near the wall the calculated temperature with thermal dispersion is lower than those without thermal dispersion; this behavior reverses away from the wall.

The effects of non-uniform porosity and thermal dispersion on streamlines (left) and isotherms (right) at $Ra_f = 10^6$ and $\gamma = 0.268$ ($d_p = 3$ mm) are illustrated in Fig. 11. With both non-uniform porosity and thermal dispersion effects taken into consideration, the strength of the vortices is the largest and the thermal energy is dispersed further away from the heated cylinder.

5. COMPARISON WITH HIMASEKHAR AND BAU'S RESULTS [5]

As mentioned earlier, Himasekhar and Bau [5] have performed a numerical and experimental investigation for natural convection from a horizontal cylinder at constant heat flux embedded in a rectangular porous box, which was insulated from three sides but not the top surface. Their numerical simulation is based on Darcy's law with constant porosity and without thermal dispersion taken into consideration.

The accuracy of the present numerical code can be assessed by comparing Himasekhar and Bau's computed Nusselt numbers with those based on the present code. To this end, the formulation of the problem presented in Sections 2–4 has to be modified as follows. First of all, Darcy's law instead of equation (3) is used as the momentum equation. Secondly, the porosity is assumed to be constant. Thirdly, the thermal boundary conditions at the walls must be changed while the no-slip boundary condition on the walls cannot be imposed. Fourthly, the governing equations are expressed in terms of stream function and temperature while the vorticity function is not needed. The computed average Nusselt numbers $\overline{Nu}_i$ (on the cylinder) and $\overline{Nu}_0$ (on the top surface of the box) based on the modified code for $Ra_m = 50$ with a grid of 65×70 points in the transformed plane are tabulated in Table 3. It is shown that these results are in excellent agreement with the numerical results obtained by Himasekhar and Bau [5], who used a grid of 50×50 points in the transformed plane.

A numerical solution was also obtained for natural convection about a horizontal cylinder with constant heat flux embedded in a porous medium with non-uniform porosity and thermal dispersion effects taken into consideration. For this case, the mathematical formulation is similar to those discussed in Sections 2 and 3, except that the thermal boundary condition at the cylinder is changed from constant wall temperature to the constant heat flux conditions. Computations were carried out corresponding to Himasekhar and Bau's experimental conditions. A comparison of numerical results based on the modified code with Himasekhar and Bau's data for $r_d = 13.9$ and $r_s = 14.6$ at four values of R_{eff} (see ref. [5] for the definitions of r_d, r_s, and R_{eff}) is presented in Table 4. It is shown that the computed Nusselt numbers with variable porosity and thermal dispersion effects taken into consideration agree the best with experimental data.

6. CONCLUDING REMARKS

In this paper, various effects on natural convection about a heated horizontal cylinder in an enclosed porous medium are investigated numerically using a body-fitted curvilinear coordinate system. The following conclusions can be drawn from the present study.

(1) The time in reaching steady state increases as the Rayleigh number is decreased.

(2) The variable porosity effect is negligible for small time and its influence increases with the particle diameter and Rayleigh number.

(3) The non-uniform porosity effect at the wall tends to increase the temperature gradient adjacent to the wall while the thermal dispersion effect increases

Table 4. Comparison of the calculated Nusselt numbers with Himasekhar and Bau's data [5]

Re_{ff}	Present code: Constant porosity, Darcy's law without dispersion	Present code: Variable porosity without dispersion, no-slip	Present code: Variable porosity with dispersion, no-slip	Himasekhar and Bau's data [5]
10	1.45	1.72	2.24	1.93†
50	2.34	2.75	3.53	3.15†
100	2.93	3.48	4.24	4.02†
700	5.59	7.42	8.62	8.10†

† These values are read from Fig. 10 in ref. [5].

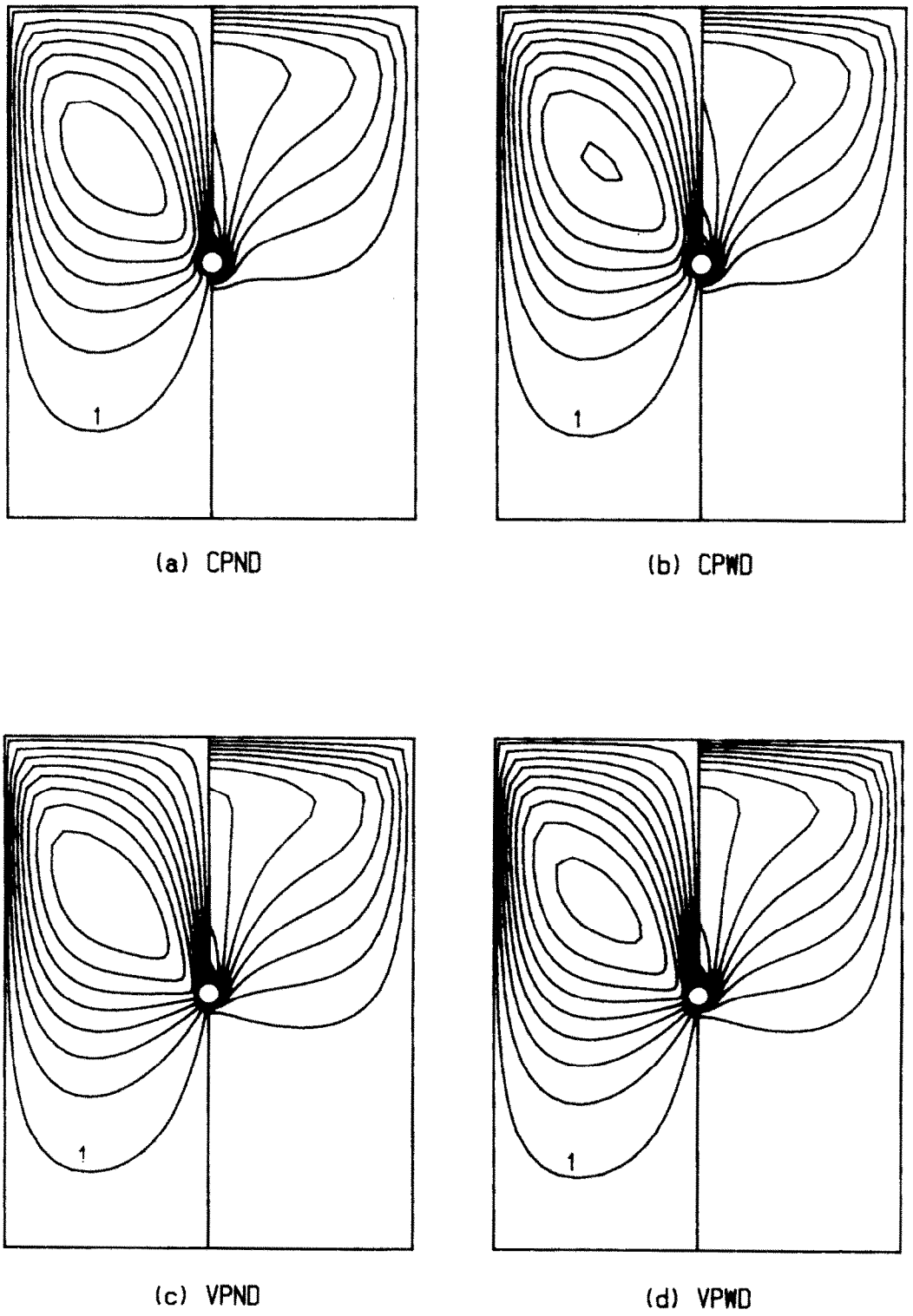

FIG. 11. Isotherms (right) and streamlines (left) for steady natural convection about a horizontal cylinder embedded in a porous cavity at $Ra_t = 10^6$ and $\gamma = 0.268$.

the thermal conductivity; both of these effects result in the enhancement of surface heat flux.

(4) The thermal dispersion effect on natural convection in a porous medium is small at low to moderate Rayleigh numbers.

(5) The predicted Nusselt numbers with variable porosity and thermal dispersion effect taken into consideration simultaneously agree better with experimental data.

REFERENCES

1. J. H. Merkin, Free convection boundary layers on axisymmetric and two-dimensional bodies of arbitrary shape in saturated porous medium, *Int. J. Heat Mass Transfer* **22,** 1461–1462 (1979).
2. P. Cheng, Natural convection in porous media: external flows. In *Natural Convection: Fundamentals and Applications* (Edited by S. Kakac, W. Aung and R. Viskanta), pp. 475–513. Martinus Nijhoff, The Hague, The Netherlands (1985).
3. R. T. Fernandez and V. E. Schrock, Natural convection from cylinders buried in a liquid-saturated porous medium, *Proc. Int. Heat Transfer Conf.*, Munich, Vol. 2, pp. 335–340 (1982).
4. R. M. Fand, T. E. Steinberger and P. Cheng, Natural convection heat transfer from a horizontal cylinder embedded in a porous medium, *Int. J. Heat Mass Transfer* **29,** 119–133 (1986).
5. K. Himasekhar and H. H. Bau, Thermal convection around a heated source embedded in a box containing a saturated porous medium, *J. Heat Transfer* **110,** 649–653 (1988).
6. J. T. Hong, Y. Yamada and C. L. Tien, Effects of non-Darcian and nonuniform porosity on vertical plate natural convection in porous media, *J. Heat Transfer* **109,** 356–362 (1987).
7. E. David, G. Lauriat and P. Cheng, Natural convection in rectangular cavities filled with variable porosity media. Presented at the *Int. Symp. on Convection in Porous Media: NonDarcy Effects* (24–27 July 1988).
8. C. T. Hsu and P. Cheng, Closure schemes of the macroscopic energy equation for convective heat transfer in porous media, *Int. Commun. Heat Mass Transfer* **15,** 689 (1988).
9. C. T. Hsu and P. Cheng, Thermal dispersion in porous media, *Int. J. Heat Mass Transfer* **33,** 1587–1597 (1990).
10. D. Vortmeyer and J. Schuster, Evaluation of steady flow profiles in rectangular and circular packed beds by a variational method, *Chem. Engng Sci.* **38,** 1691–1699 (1983).
11. M. L. Hunt and C. L. Tien, Non-Darcian convection in cylindrical packed beds, *J. Heat Transfer* **110,** 378–384 (1988).
12. P. Cheng, A. Chowdhury and C. T. Hsu, Forced convection in packed tubes and channels with variable porosity and thermal dispersion effects, *Proc. NATO Advanced Study Institute on Convective Heat and Mass Transfer in Porous Media*, pp. 361–404 (1990).
13. S. Ergun, Fluid flow through packed columns, *Chem. Engng Prog.* **48,** 89–94 (1952).
14. I. F. Macdonald, M. S. El-Sayed, K. Mow and F. A. Dullien, Flow through porous media—The Ergun equation revisited, *Ind. Engng Chem. Fundam.* **18,** 199–207 (1979).
15. R. M. Fand, B. Y. Kim, A. C. C. Lam and R. T. Phan, Resistance to the flow of fluids through simple and complex porous media whose matrices are composed of randomly packed spheres, *J. Fluid Engng* **109,** 268–274 (1987).
16. P. Zehner and E. U. Schluender, Waermeleitfa-higkeit von Schuettungen bei Massigen Temperaturen, *Chem.-Ing.-Tech.* **42,** 933–941 (1970).
17. R. M. Fand and R. T. Phan, Combined forced and natural convection heat transfer from a horizontal cylinder embedded in a porous medium, *Int. J. Heat Mass Transfer* **30,** 1351–1358 (1987).
18. J. F. Thompson, F. C. Thames and C. W. Mastin, Automatic numerical generation of body-fitted curvilinear coordinate system for field containing any number of arbitrary two-dimensional bodies, *J. Comput. Phys.* **15,** 299–319 (1974).
19. J. F. Thompson, F. C. Thames and C. W. Mastin, TOMCAT—a code for numerical generation of boundary fitted curvilinear coordinate systems of fields containing any number of arbitrary two-dimensional bodies, *J. Comput. Phys.* **24,** 274–302 (1977).
20. J. F. Middlecoff and P. D. Thomas, Direct control of the grid point distribution in meshes generated by elliptic equations, *AIAA J.* **18,** 652–656 (1980).